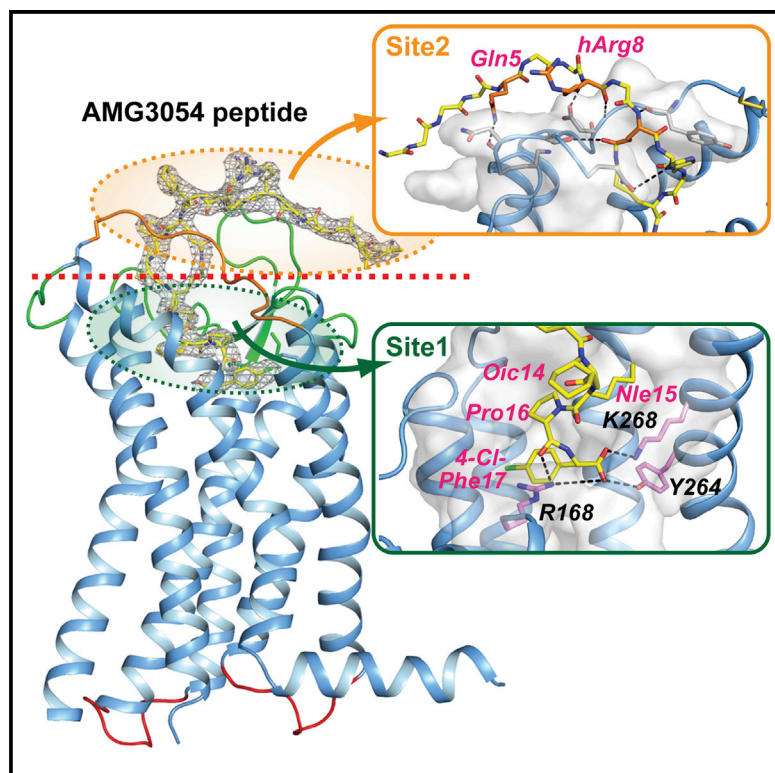


# Structure

## Structural Basis for Apelin Control of the Human Apelin Receptor

### Graphical Abstract



### Authors

Yingli Ma, Yang Yue, Yanbin Ma, ...,  
Wenge Zhong,  
Mingqiang Zhang, Fei Xu

### Correspondence

xufei@shanghaitech.edu.cn

### In Brief

Ma et al. present an atomic-resolution structure of the human apelin receptor (APJR, a class A G-protein-coupled receptor) in complex with a 17-residue apelin peptide mimic by X-ray crystallography. This structure reveals a two-site ligand binding mode that has not been seen in any other solved class A receptor structures.

### Highlights

- Designed peptide mimic AMG3054 with reduced conformational flexibility
- Structure of apelin receptor in complex with AMG3054
- Designed peptide AMG3054 adopts a lactam constrained curved structure
- A two-site binding mode is observed for peptide GPCR recognition



# Structural Basis for Apelin Control of the Human Apelin Receptor

Yingli Ma,<sup>1</sup> Yang Yue,<sup>2</sup> Yanbin Ma,<sup>1</sup> Qing Zhang,<sup>1</sup> Qingtong Zhou,<sup>2</sup> Yunpeng Song,<sup>1</sup> Yuqing Shen,<sup>1</sup> Xun Li,<sup>1</sup> Xiaochuan Ma,<sup>1</sup> Chao Li,<sup>2,3,4,5</sup> Michael A. Hanson,<sup>6</sup> Gye Won Han,<sup>7</sup> E. Allen Sickmier,<sup>8</sup> Gayathri Swaminath,<sup>9</sup> Suwen Zhao,<sup>2,3</sup> Raymond C. Stevens,<sup>2,3</sup> Liaoyuan A. Hu,<sup>1</sup> Wenge Zhong,<sup>1</sup> Mingqiang Zhang,<sup>1</sup> and Fei Xu<sup>2,3,10,\*</sup>

<sup>1</sup>Amgen Asia R&D Center, Amgen Biopharmaceutical R&D (Shanghai) Co., Ltd

<sup>2</sup>iHuman Institute, ShanghaiTech University, 2F Building 6, 99 Haike Road, Pudong New District

<sup>3</sup>School of Life Science and Technology, ShanghaiTech University  
Shanghai 201210, China

<sup>4</sup>Institute of Biochemistry and Cell Biology, Shanghai Institutes for Biological Sciences, Chinese Academy of Sciences,  
Shanghai 200031, China

<sup>5</sup>University of Chinese Academy of Sciences, Beijing 100049, China

<sup>6</sup>GPCR Consortium, San Marcos, CA 92078, USA

<sup>7</sup>Department of Chemistry, Bridge Institute, University of Southern California, Los Angeles, CA 90089, USA

<sup>8</sup>Therapeutic Discovery, Department of Molecular Engineering, Amgen Inc., 360 Binney Street, Cambridge, MA 02142, USA

<sup>9</sup>Cardiovascular Disorders, Amgen Inc., 1120 Veterans Boulevard, South San Francisco, CA 94080, USA

<sup>10</sup>Lead Contact

\*Correspondence: [xufei@shanghaitech.edu.cn](mailto:xufei@shanghaitech.edu.cn)

<http://dx.doi.org/10.1016/j.str.2017.04.008>

## SUMMARY

Apelin receptor (APJR) is a key regulator of human cardiovascular function and is activated by two different endogenous peptide ligands, apelin and Elabela, each with different isoforms diversified by length and amino acid sequence. Here we report the 2.6-Å resolution crystal structure of human APJR in complex with a designed 17-amino-acid apelin mimetic peptide agonist. The structure reveals that the peptide agonist adopts a lactam constrained curved two-site ligand binding mode. Combined with mutation analysis and molecular dynamics simulations with apelin-13 binding to the wild-type APJR, this structure provides a mechanistic understanding of apelin recognition and binding specificity. Comparison of this structure with that of other peptide receptors suggests that endogenous peptide ligands with a high degree of conformational flexibility may bind and modulate the receptors via a similar two-site binding mechanism.

## INTRODUCTION

The apelin receptor (the angiotensin receptor like-1, the angiotensin II protein J receptor, or APJR), a member of the class A  $\gamma$ -group of G-protein-coupled receptors (GPCRs), is involved in diverse (patho)physiological functions such as angiogenesis, vasoconstriction, heart muscle contractility, regulation of energy metabolism, and fluid homeostasis (Masri et al., 2005; O'Carroll et al., 2013; Pitkin et al., 2010). Human genetic studies demonstrated that polymorphisms of APJR genes were associated with increased risks of hypertension and coronary artery dis-

eases (Falcone et al., 2012; Kadoglou et al., 2010). APJR was cloned in 1993 (O'Dowd et al., 1993) and subsequently orphanized with the discovery of its first endogenous ligand apelin, followed by the recent discovery of its second endogenous ligand Elabela (ELA)/Toddler/Apela (Chng et al., 2013; Pauli et al., 2014). These endogenous peptide ligands of APJR vary in length and amino acid sequence. Apelin peptides of multiple lengths (apelin-36, -17, and -13) result from maturation and proteolysis from the same prepropeptide. Despite the apparent lack of sequence similarity, previous studies reported that apelin and ELA peptides occupy the same orthosteric binding site on APJR and both activate the receptor through the  $G_{i/o}$  pathway, as well as  $\beta$ -arrestin1/2 recruitment (Murza et al., 2016). The therapeutic potential of APJR agonists for cardiac diseases was evaluated in a clinical study which demonstrated that acute administration of apelin in heart-failure patients significantly improved overall cardiac functions (Japp et al., 2010). Thus, to understand the fundamental biology, we sought to gain structural insights into the molecular basis of APJR-peptide recognition and receptor signal transduction. Here we report the crystal structure of human APJR in complex with a designed apelin-17 mimetic peptide.

## RESULTS

### Structural Determination of the Agonist Peptide-Bound APJR Complex

The expression level of wild-type (WT) full-length APJR was extremely low and the protein was not amenable for structural studies. To overcome this challenge and obtain high-quality crystals, especially in the presence of a peptide agonist, we designed a construct with improved yield, monodispersity, and thermostability. Residues were truncated from both the N (residues 1–6) and C termini (residues 331–380). Rubredoxin (residues 1–54) (Chun et al., 2012) was inserted between A229 and R243 to replace most of intracellular loop 3 (ICL3).

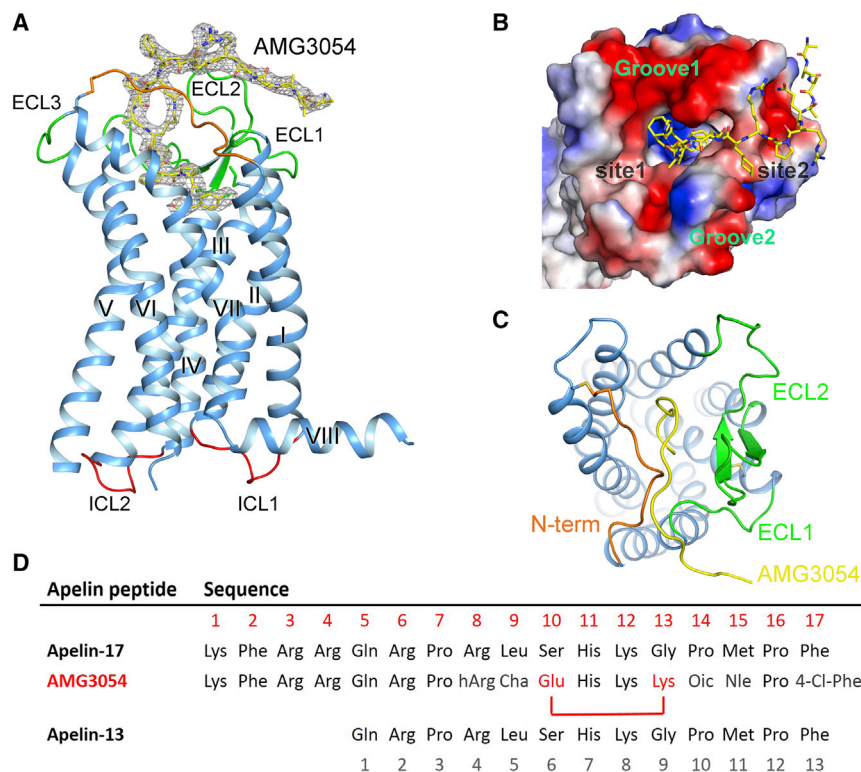


### Figure 1. Overall Structure and Peptide Ligand Alignment of APJR-AMG3054

(A) Side view of overall APJR-AMG3054 structure. AMG3054 is shown as sticks in meshed electron density map ( $2F_o - F_c$ ,  $\sigma = 1.0$ ) (A) or cartoon (B and C) in yellow color. APJR is represented as cartoon in blue color. Transmembrane helices are text labeled; extracellular and intracellular loops are indicated in green and red colors, respectively. Disulfide bonds are shown as yellow lines.

(B) Peptide AMG3054 is highlighted as yellow sticks, with APJR represented as surface colored by electrostatic properties. AMG3054 central binding site 1 and surface binding site 2 are labeled. The additional two surface grooves are labeled as Groove 1 and Groove 2.

(C) APJR is presented as a blue cartoon with the N-term loop (orange), ECL2 loop (green), and ECL1 loop (green), respectively. AMG3054 is colored in yellow as cartoon.

(D) Multiple sequence alignment of apelin-17, AMG3054, and apelin-13. Discrepant residues among the peptides are colored in red. hArg, Cha, Oic, Nle and 4-Cl-Phe are unnatural amino acid counterparts. The lactam ring is highlighted in red. Numbering for the peptide is indicated in red for apelin-17 and AMG3054, and gray for apelin-13. See also [Figures S1–S4](#) and [Table S1](#).

We introduced two C-terminal mutations C325L and C326M to remove the palmitoylation sites and T177N in extracellular loop 2 (ECL2) to remove an N-glycosylation site. Furthermore, we introduced two additional mutations, V117<sup>3.40</sup>A and W261<sup>6.48</sup>K (superscripts indicate Ballesteros-Weinstein numbering [Ballesteros and Weinstein, 1995]), through computer-aided design and extensive mutation screening (Figure S1). The combination of these five mutations helped to greatly improve the protein yield, homogeneity, and stability (Figure S1). To decrease the conformational flexibility of apelin and to form a more stable interaction with APJR (Langelaan et al., 2009), we designed a series of conformationally constrained cyclic peptides. These peptides were assessed by thermal stability with the receptor, and the best candidate from this effort was the 17-mer AMG3054 with a lactam formed between the side chains of Glu10 and Lys13 (Figure 1D). This engineered APJR construct was co-crystallized with AMG3054, and the structure was solved at 2.6-Å resolution by molecular replacement. Details of data collection and refinement are provided in [Table S1](#).

### Overall Architecture of APJR-AMG3054

The refined structure contains receptor residues 19–330 with the segment of residues 230–242 within ICL3 replaced by rubredoxin. All the extracellular loops are well modeled, except for the short N-terminal fragment (containing residues 7–18), which is disordered in the structure (Figures 1A and S1). The two conserved disulfide bonds within the class A peptide GPCR family C19<sup>N-term</sup>-C281<sup>ECL3</sup> and C102<sup>3.25</sup>-C181<sup>ECL2</sup> hold the extracellular loops and transmembrane helices in registry (Figure 1A).

The APJR-AMG3054 complex structure reported here shows a typical seven-transmembrane helical bundle arrangement

that shares a similar overall architecture as that previously reported for other class A GPCRs in the  $\beta$  and  $\gamma$  groups ( $\mu$ -opioid receptor [OR] (Manglik et al., 2012),  $\delta$ -OR (Fenalti et al., 2014; Granier et al., 2012),  $\kappa$ -OR (Wu et al., 2012), CXCR4 chemokine receptor (Wu et al., 2010), angiotensin II type 1 receptor (AT1R) (Zhang et al., 2015), neurotensin receptor NTSR1 (White et al., 2012) and endothelin receptor type B (ETbR) (Shihoya et al., 2016)) (Figure S2). When compared with other antagonist-bound  $\gamma$ -group GPCR structures and both the active and inactive  $A_{2A}$  adenosine receptor ( $A_{2A}$ AR) structures (Carpenter et al., 2016; Jaakola et al., 2008; Xu et al., 2011), APJR presents an inactive-like conformation (Figure S3A). This is not altogether surprising given that we mutated two of the highly conserved residues (V117<sup>3.40</sup>A and W261<sup>6.48</sup>K) involved in receptor activation (Caltabiano et al., 2013; Shi et al., 2002; Smit et al., 2007). Main-chain atoms of V117<sup>3.40</sup> and W261<sup>6.48</sup> are located about 11 Å away from the orthosteric agonist binding site and the single mutations V117<sup>3.40</sup>A or W261<sup>6.48</sup>K maintained WT level binding and signaling activity by apelin-13. However, the combined mutations greatly diminished binding to apelin-13 (Figures S3B and S3C).

On the extracellular side, three relatively shallow grooves (Figure 1B) are visually identifiable on the receptor's surface. We define these as groove 1 (D172, E174, D184, and E194, all in ECL2), groove 2 (D282<sup>7.26</sup> and surrounding region), and a third groove that is directly involved in peptide ligand binding and subsequently identified as "site 2." Site 2 is formed on one side by the receptor's N-terminal loop which is anchored by the C19<sup>N-term</sup>-C281<sup>ECL3</sup> disulfide bond. This disulfide bond between N-terminal loop and the tip of helix VII stabilizes the otherwise disordered N-terminal loop in a well-defined conformation.

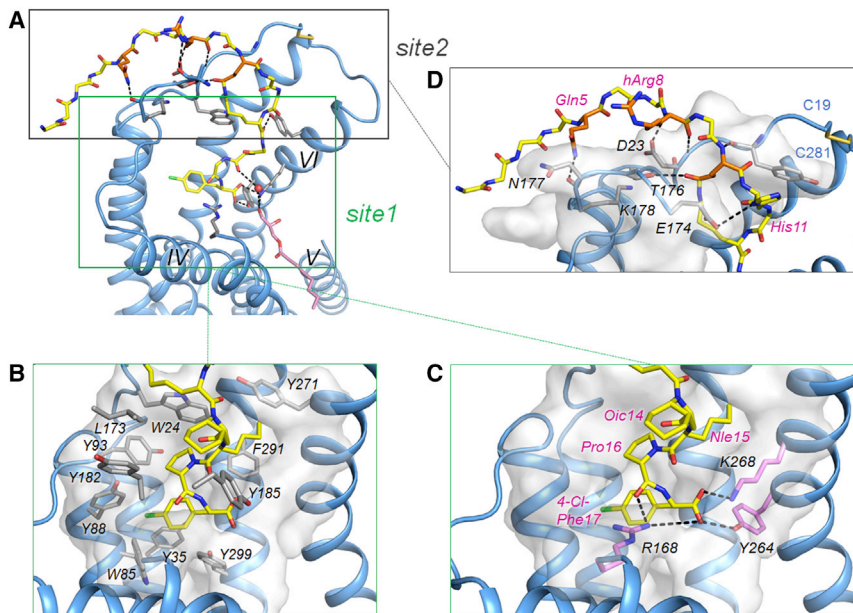


**Figure 2. Two-Site Binding Mode of AMG3054**

(A) Major backbone and side-chain interactions between AMG3054 and APJR. For clarity, only the main chain of AMG3054 is shown in yellow sticks with residues engaged in side-chain interactions highlighted in orange. Key APJR residues that are engaged in the interaction network are shown as gray (for side-chain interaction) or blue (for main-chain interaction) sticks. Polar or non-polar interactions between peptide and APJR are indicated by black dashed lines. Part of APJR's helices and loops were removed for clarity. A water molecule mediating the interaction network between AMG3054, APJR, and the lipid (OLC) is shown as a red sphere.

(B) Major hydrophobic interactions between APJR site 1 and AMG3054 are highlighted. Key residues in site 1 are shown as gray sticks and labeled in black. AMG3054 residues are shown as yellow sticks.

(C) Major polar interactions between APJR site 1 and AMG3054 are indicated by black dashed lines. Key residues that are engaged in site 1 polar interactions are shown as pink sticks and labeled in black. AMG3054 residues are shown as yellow sticks and labeled in magenta.

(D) Major polar interactions between APJR site 2 and AMG3054 are indicated by black dashed lines. Key residues that are engaged in site 2 polar interactions are shown as gray sticks and labeled in black. AMG3054 residues are shown as yellow sticks and labeled in magenta.

See also [Figure S4](#).

On the other side of site 2, the long ECL2 forms an ordered  $\beta$ -hairpin motif, as has been observed in other GPCRs ([Figure S2](#)), but makes distinct non-polar and hydrogen-bonding interactions with AMG3054 ([Figure 2](#)).

### Two-Site Ligand Binding Mode

The most remarkable feature of the APJR-AMG3054 complex structure is that the bound apelin-17 mimetic peptide AMG3054 adopts a curved binding conformation, binding to APJR through a two-site binding mode. Five amino acids at the C-terminal end of the peptide bind deeply into the canonical ligand binding pocket, which is approximately perpendicular to the membrane plane. For discussion purposes in this article, we term this canonical orthosteric site “site 1.” The lactam ring formed by the side chains of Lys13 and Glu10 (amino acids of the peptide ligand are denoted by their three-letter code throughout this article) ([Figure 1D](#)) in the ligand causes the peptide main chain to bend by about  $90^\circ$  from its membrane-perpendicular direction, and projects the N-terminal half of the peptide outside of “site 1” into one of the surface grooves, which we termed “site 2” as discussed above ([Figures 1B](#) and [2A](#)). This two-site binding mode has not been observed previously for any of the peptide GPCR co-crystal structures.

As shown in [Figure 2C](#), the C-terminal residues of AMG3054 bind to site 1 through hydrophobic and polar interactions ([Figures 2B](#) and [2C](#)). The side chain of 4-Cl-Phe17 makes van der Waals contacts with a large hydrophobic cavity that is delineated by the side chains of Y35<sup>1.39</sup>, W85<sup>2.60</sup>, Y88<sup>2.63</sup>, Y93<sup>ECL1</sup>, and Y299<sup>7.43</sup> ([Figure 2B](#)). While the pyrrole ring of Pro16 binds in another small hydrophobic region bordered by W24<sup>N-term</sup> and Y93<sup>ECL1</sup>, it induces a sharp kink in the peptide to sandwich the aliphatic side chain of Nle15 between the aromatic side chains

of Y271<sup>6.58</sup> and F291<sup>7.35</sup>. Oic14 forms additional hydrophobic interactions with L173<sup>ECL2</sup>, Y182<sup>ECL2</sup>, and Y185<sup>ECL2</sup>. The most important polar interactions at site 1 enlist an intricate network of salt bridges and hydrogen bonds that are formed by the terminal carboxyl group of 4-Cl-Phe17, the side-chain  $\epsilon$ -amino group of K268<sup>6.55</sup>, and the side-chain phenolic OH group of Y264<sup>6.51</sup>. The side chain of R168<sup>ECL2</sup> also engages in a potential hydrogen bond with the main chain carbonyl of Pro16 and an electrostatic interaction of the carboxyl of 4-Cl-Phe17 ([Figure 2C](#)). These general hydrophobic and polar interactions form the basic framework for ligand binding at site 1 and explain the findings that the C-terminal residues of the peptide ligand are critical for binding affinity, specificity, and biological function in numerous structure-activity relationship (SAR) studies ([Medhurst et al., 2003](#); [Murza et al., 2012](#))\_ENREF\_18.

Comparison of the APJR-AMG3054 structure with the currently available structures of GPCR-peptide complexes shows that site 1 shares a similar overall depth with the identified peptide binding sites in these complexes ([Figure S2](#)). The volume of the peptide binding sites, however, is quite diverse. APJR and NTR1 peptide sites are similar in volume while peptide sites in CXCR4 and ETbR are much larger. The volume diversity may reflect the flexibility in peptide recognition across peptide GPCRs. More available GPCR structures and follow-up peptide pocket studies will enhance our understanding in this regard.

At the kink of the curved peptide constrained by the side-chain lactam ring, polar interactions, including a potential hydrogen bond between lactam C=O and the side chain of T176<sup>ECL2</sup> and a possible electrostatic interaction between His11 and E174<sup>ECL2</sup>, help to hold the peptide in place ([Figure 2D](#)). The N-terminal half of AMG3054 binds as an extended form at site 2 through shape and non-specific electrostatic potential

**Table 1. [<sup>125</sup>I]Apelin Binding Assay of Mutant APJR Receptors<sup>a</sup>**

Mutated Residues	B-W Numbering	Binding Site Location	Mean K <sub>D</sub> (nM)	SEM K <sub>D</sub> (nM)	Mean AP13 cAMP EC <sub>50</sub> (M)	SEM AP13 cAMP EC <sub>50</sub> (M)
WT			0.05	0.005	4.0 × 10 <sup>-10</sup>	6.6 × 10 <sup>-11</sup>
Y35A	1.39	site 1	NBD <sup>b</sup>	NBD	–	–
W85A	2.60	site 1	NBD	NBD	–	–
R168A	ECL2	site 1	NBD	NBD	–	–
Y264F	6.51	site 1	0.12	0.011	2.0 × 10 <sup>-10</sup>	3.8 × 10 <sup>-11</sup>
K268A	6.55	site 1	0.16	0.017	1.0 × 10 <sup>-9</sup>	1.7 × 10 <sup>-10</sup>
Y271A	6.58	site 1	NBD	NBD	>1.0 × 10 <sup>-8</sup>	–
D23A	N term	site 2	0.22	0.013	3.9 × 10 <sup>-9</sup>	1.4 × 10 <sup>-9</sup>
D284A	7.28	site 2	NBD	NBD	>1.0 × 10 <sup>-8</sup>	–
D172A	ECL2	groove 1	0.09	0.006	5.5 × 10 <sup>-10</sup>	1.1 × 10 <sup>-10</sup>
E174A	ECL2	groove 1	0.07	0.012	4.9 × 10 <sup>-10</sup>	9.4 × 10 <sup>-11</sup>
D184A	ECL2	groove 1	0.22	0.024	7.9 × 10 <sup>-10</sup>	8.1 × 10 <sup>-11</sup>
E194A	ECL2	groove 1	0.12	0.003	1.2 × 10 <sup>-9</sup>	6.2 × 10 <sup>-10</sup>

<sup>a</sup>Data are presented as Mean and SEM of three or more independent experiments. B-W, Ballesteros-Weinstein; cAMP, cyclic AMP.

<sup>b</sup>NBD, no binding detected.

complementarity. There is a short anti-parallel  $\beta$  sheet formed between hArg8-Glu10 and Y21<sup>N-term</sup>-D23<sup>N-term</sup>, supported by two main-chain hydrogen bonds, C=O of hArg8 to N-H of D23<sup>N-term</sup> and N-H of Glu10 to C=O of Y21<sup>N-term</sup>, respectively. hArg8 contributes additional binding via another hydrogen-bonding interaction between its main-chain amide N-H and the side chain of D23<sup>N-term</sup>. K178<sup>ECL2</sup> orients its side chain toward the site 2 pocket and mediates an extensive peptide receptor interaction network, pulling ECL2 into close contact with the peptide. Gln5 of the peptide projects toward T177<sup>ECL2N</sup>, and a short hydrogen bond (2.7 Å) is observed between the side chain of Gln5 and the C=O of T177<sup>ECL2N</sup>, augmenting the peptide interaction with ECL2. These structural details of site 2's interactions support previous SAR analysis that the QRPR motif in apelin's N terminus is important for binding affinity and ligand activity (Medhurst et al., 2003). Indeed, apelin-13, the shorter version of the endogenous apelin peptide, which lacks the first four amino acids and begins with the QRPR motif (starting at Gln5 of apelin-17), has been reported to have comparable binding affinity with the longer apelin-17 and apelin-36 (Chandrasekaran et al., 2008). When tested, a truncated version of the AMG3054 peptide starting at Arg6 elicited full functional activity compared with AMG3054. However, additional truncation of the N-terminal residues of AMG3054 causes near complete loss of functional activity, providing additional evidence for the critical importance of site 2 in ligand activity (Figure S4).

We performed alanine mutagenesis for the key residues at sites 1 and 2 in APJR that are involved in AMG3054 binding to the receptor, and examined the effects of these single mutations on <sup>125</sup>I-labeled apelin-13 binding and signaling. At site 1, while K268<sup>6.55</sup>A exhibited a slightly reduced binding affinity, W85<sup>2.60</sup>A exhibited a dramatically detrimental effect; R168<sup>ECL2</sup>A and Y271<sup>6.58</sup>A completely abolished the binding of apelin-13 (Table 1). At site 2, D23<sup>N-term</sup>A exhibited a 5-fold reduction in binding affinity (Table 1). Together, these mutagenesis data suggested that the critical interactions identified from the APJR-AMG3054 complex structure are also important for apelin

peptide binding to APJR, providing compelling evidence that apelin binds to APJR via the same two-site binding mode.

### Molecular Dynamics Simulations of Apelin-13 Binding Mode to WT APJR

To gain more comprehensive insights into how the endogenous apelin peptide ligands bind to APJR, we performed restraint-free molecular dynamics (MD) simulations of the apelin-13 peptide in complex with WT APJR which does not contain any truncations, fusion insertions, or mutations. Alignment of the resulting final MD model with the experimental APJR crystal structure showed a conformation that was consistent overall with a root-mean-square deviation at 2 Å (Figure 3A). The model revealed a curved two-site binding pose for apelin-13 that was almost identical to that of the crystal structure; site 1 is quite stable, while site 2 is relatively more flexible with fewer constraints. Similar to AMG3054, apelin-13 interacts with the receptor mainly through hydrophobic shape complementarity and polar side-chain to side-chain and to main-chain interactions (Figures 3B and 3C). At the bottom of site 1, in addition to the expected hydrophobic van der Waals interactions, the carboxyl group of Phe13 (sequence numbering according to apelin-13, Figure 1D) makes hydrogen-bonding interactions with K268<sup>6.55</sup> and Y264<sup>6.51</sup>. This is consistent with AMG3054 where the carboxyl group of 4-Cl-Phe17 leans to K268<sup>6.55</sup> and Y264<sup>6.51</sup> on helix VI as well. The key interactions contributed by carboxyl group and main chain of the peptide are supported by the peptide SAR data that Phe13Ala does not affect the binding affinity, yet truncation of Phe13 reduces binding, and truncation of both Pro12 and Phe13 completely abolished binding (Fan et al., 2003; Zhang et al., 2014). Interestingly, a cluster of aromatic residues, W24<sup>N-term</sup>, W85<sup>2.60</sup>, Y88<sup>2.63</sup>, Y93<sup>ECL1</sup>, W195<sup>ECL2</sup>, Y264<sup>6.51</sup>, Y271<sup>6.58</sup>, F291<sup>7.35</sup>, and Y299<sup>7.43</sup>, form a hydrophobic pocket to embrace the C terminus of the apelin-13 peptide and contribute to the extremely stable interaction network in site 1.

The most noticeable differences between the apelin-13 binding model and our APJR-AMG3054 crystal structure, which

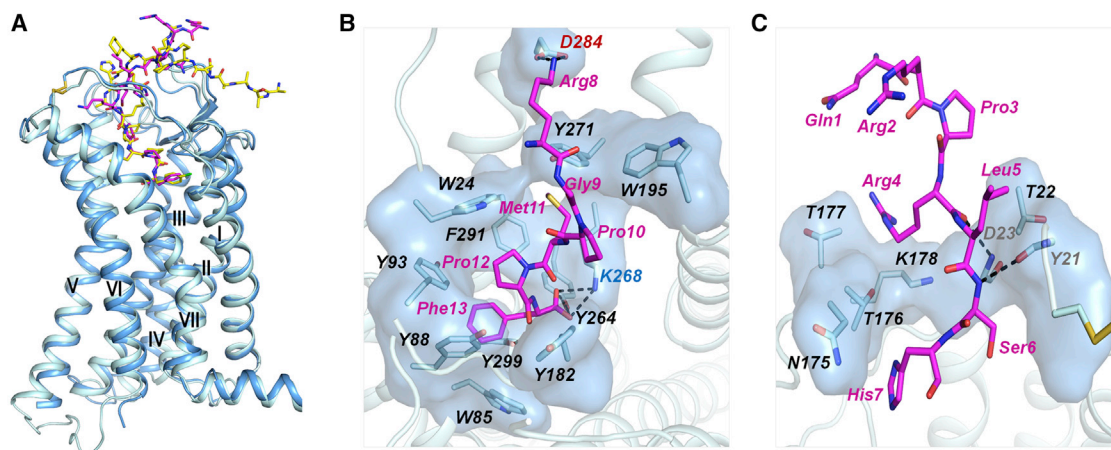


**Figure 3. Apelin-13 Binding Pose in WT APJR**

(A) Superposition of WT APJR/Apelin-13 MD model (cyan sticks for the receptor and magenta sticks for apelin-13 peptide) with the crystal structure of APJR-AMG3054 complex (blue cartoon for the receptor and yellow sticks for AMG3054).

(B) Ligand-receptor binding interactions in site 1. Apelin-13 residues are labeled with magenta text; receptor residues are labeled in blue (for basic residues), red (for acidic residues), and black (for other residues); and site 1 is shown as a surface. Polar contacts are indicated by black dashed lines.

(C) Ligand-receptor binding interactions in site 2. Apelin-13 and receptor residues are labeled with magenta and black text, respectively. Site 2 is shown as a surface. Polar contacts are indicated by black dashed lines.

See also Figure S3.

nonetheless contribute to maintaining the same overall binding mode, stem from peptide sequence differences. Without a lactam ring as in AMG3054, apelin-13 approaches site 2 binding through an important polar interaction between Lys8 and D284<sup>7,28</sup> at the junction of site 1 and site 2 (Figure 3B). Consistent with this structural insight, a Lys8Ala mutation on apelin-13 dramatically reduced the peptide's binding affinity (Fan et al., 2003; Zhang et al., 2014), and the D284<sup>7,28</sup>A mutation on APJR caused a complete loss of [<sup>125</sup>I]apelin-13 binding (Table 1).

## DISCUSSION

### The Two-Site Peptide Ligand Binding Mode

We evaluated the possibility that the two-site binding mode could be used to explain a general binding mode for other class A peptide GPCRs (e.g., opioid receptors). The endogenous peptide ligands of the three major subtypes of opioid receptors are of similar length as apelin peptides (Janecka et al., 2004). Pioneering peptide SAR research in the 1970s and 1980s led to the “message-address” hypothesis for peptide ligand binding, specificity, and functional activity (Schwyzer, 1977). The co-crystal structures of all three opioid receptors have been published to date (Fenalti et al., 2014; Granier et al., 2012; Manglik et al., 2012; Wu et al., 2012), and recently binding models of dynorphin A(1–13) to the  $\kappa$ -opioid receptor ( $\kappa$ -OR) were proposed based on a solution nuclear magnetic resonance study of the dynorphin peptide conformation in the presence of  $\kappa$ -OR (O'Connor et al., 2015). However, a complex structure of such a receptor with a cognate peptide ligand has yet to be reported, and thus no direct structural evidence of the binding mode for the full-length peptide ligand is currently available.

We therefore examined the complex of  $\kappa$ -OR with its endogenous ligand dynorphin A as a representative system via mo-

lecular modeling. Based on the published  $\kappa$ -OR-dynorphin A(1–13) model (O'Connor et al., 2015), we generated a  $\kappa$ -OR-dynorphin A(1–17) model (Figure 4) using the insights from our APJR-AMG3054 structure, the available  $\kappa$ -OR mutagenesis studies, and dynorphin SAR data (Chavkin and Goldstein, 1981; Vardy et al., 2013). In the model, the ligand dynorphin A(1–17) clearly assumes a similar two-site binding mode. The “message” YGGF N-terminal segment of dynorphin binds to site 1, engaging in the expected hydrophobic,  $\pi$ -stacking, and polar interactions. Protruding out from site 1, the “address” segment of the ligand also takes a turn at the central part Leu5-Arg9, which coincides with the previous model (O'Connor et al., 2015). Several salt-bridge interactions between dynorphin and  $\kappa$ -OR (Arg6-E203 and E209, Arg7-D223 and E297, and Arg9-D204, respectively) are formed in this region, among which the importance of the Arg7-E297 interaction has been postulated previously from mutagenesis data (Vardy et al., 2013). In addition, the C-terminal part of dynorphin A interacts with  $\kappa$ -OR (Lys11-T306, Lys13-E203, Asp15-R202) in a manner that is consistent with the previous SAR data (Chavkin and Goldstein, 1981). These interactions work in concert to hold the peptide in place and guide it into site 2, binding in analogous manner as seen in the APJR-AMG3054 structure. The “message-address” hypothesis is thought to be generally applicable to a large number of class A GPCRs such as  $\mu$ -OR,  $\delta$ -OR, and the adrenocorticotropin receptors. We thus contemplate that the two-site binding mode we unveiled for APJR-AMG3054 may be also utilized by other class A GPCR endogenous peptide ligands bound to their respective receptors. We should note that depending on the specific ligand-receptor pair, the exact location of site 2 on the surfaces may be different, and this site 2 structural diversity may provide an additional structural basis for differentiated ligand binding, specificity, and function.

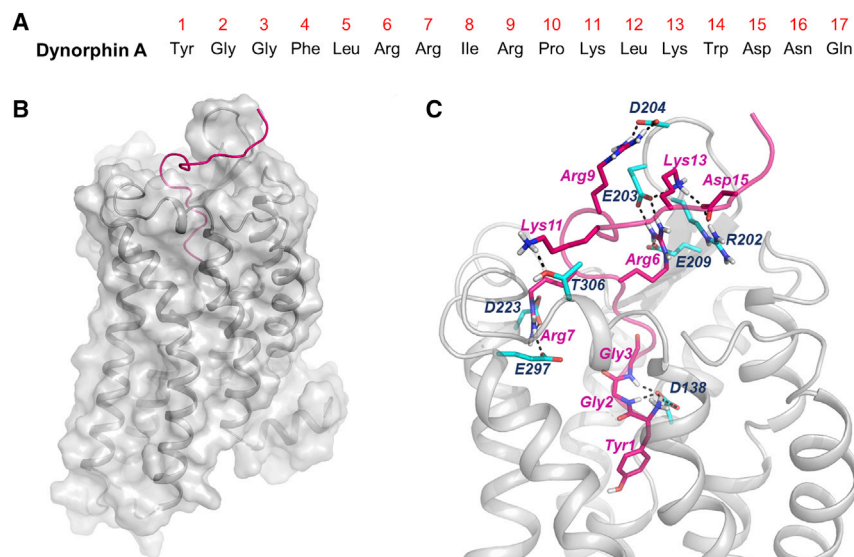


**Figure 4.  $\kappa$ -OR/Dynorphin A Complex MD Model**

(A) Sequence of dynorphin A(1–17) peptide.

(B) Overview of  $\kappa$ -OR-dynorphin A complex MD model represented as cartoon with  $\kappa$ -OR in white with surface and dynorphin A in red.

(C) Interactions between dynorphin A and  $\kappa$ -OR are presented with  $\kappa$ -OR as white cartoon with key residues as cyan sticks with blue labels. Dynorphin A is presented in red with key residues as red sticks with magenta labels. Polar contacts are indicated by black dashed lines.

See also Figure S5.

### Implications from the APJR-AMG3054 Structure

Analysis of the extracellular surface of the APJR-AMG3054 complex structure identifies two additional negatively charged grooves that are not occupied by peptide ligand (Figure 1B): groove 1 and groove 2. In agreement with the observed AMG3054 binding mode, alanine scanning mutagenesis on groove 1 residues (D172A, E174A, D184A, E194A) showed no effect on apelin-13 binding affinity (Table 1). While it is conceivable that shorter peptide agonists with 17 amino acids or less are not long enough to reach into these additional grooves, it may be that the longer endogenous peptide ligands such as apelin-36 that contain additional positively charged amino acids toward their N terminus could wind into this patch and insert their extended N-terminal sections into groove 1 through electrostatic interactions. The implication of such additional interactions is that longer peptide ligands may have a prolonged duration of action. Indeed, it is well established that apelin-36 has longer-lasting effects on APJR activation than apelin-13 (Goidescu and Vida-Simiti, 2015). In human healthy volunteers, pyr-apelin-13 produced a rapid dose-dependent increase of blood flow that reached a plateau, but the effect was reproducible after a saline washout period (Japp et al., 2010). In contrast, apelin-36 produced a more durable response that could not be recapitulated after a washout period. The possible binding at additional site(s) by apelin-36 may have other implications. A previous report indicated that APJR may be a co-receptor for HIV viral entry and infection in the brain (Choe et al., 1998; Zhou et al., 2003). We generated an APJR-HIV gp120 V3 loop complex model based on previous modeling studies of CXCR4-HIV gp120 V3 loop (Tamamis and Floudas, 2013; Wu et al., 2010). We identified multiple electrostatic interaction pairs between negatively charged groove 1 and groove 2 residues on APJR and the positively charged V3 loop that are potentially involved in mediating viral entry (Figure S5), in similar fashion to CXCR4-mediated HIV viral infection (Tamamis and Floudas, 2013). Apelin-36 blocks the infection more effectively than the shorter apelin-13, providing indirect evidence to support the

likelihood that the N-terminal segment of apelin-36 binds to APJR at additional site(s) (Zou et al., 2000).

Another interesting observation is the linear electron density in the side space between helix IV and V, which fits well with a (2R)-2,3-dihydroxypropyl-(9Z)-octadec-9-enoate (OLC) molecule that comes from lipid monoolein (Figure 2A).

This molecule is within distance to directly hydrogen bond with the C terminus of the peptide and mediates interaction to K268<sup>6,55</sup>. Further studies are necessary to understand its possible functional role in APJR agonist binding and signaling.

In the development of new therapeutics, peptide receptors in particular have often been difficult to drug because of multiple points of attachment of the peptide to the receptor. It is fascinating how peptide ligands can have such conformational flexibility in solution (Langelaan et al., 2009) and a subtle constraint can lead to a stabilized and crystallized form for receptor-ligand structural analysis. In this case, we postulate that the two-site binding mode revealed by the APJR-AMG3054 structure can be employed as one mechanism to understand the binding and recognition of peptide ligands to their respective class A peptide GPCRs, which are important targets of tremendous pharmaceutical interest.

### STAR★METHODS

Detailed methods are provided in the online version of this paper and include the following:

- KEY RESOURCES TABLE
- CONTACT FOR REAGENT AND RESOURCE SHARING
- METHOD DETAILS
  - Cloning and Expression
  - Protein Purification
  - Crystallization
  - Data Collection and Structure Determination
  - Mutagenesis and Generation of Cell Lines
  - cAMP Assay
  - APJR Saturation Binding
  - Molecular Dynamics Simulations of APJR with Endogenous Peptide Apelin-13
  - Molecular Modeling of  $\kappa$ -OR-Dynorphin A Complex
  - Molecular Modeling of APJR-gp120 V3 Loop Complex
- QUANTIFICATION AND STATISTICAL ANALYSIS
- DATA AND SOFTWARE AVAILABILITY

## SUPPLEMENTAL INFORMATION

Supplemental Information includes five figures and one table and can be found with this article online at <http://dx.doi.org/10.1016/j.str.2017.04.008>.

## AUTHOR CONTRIBUTIONS

Yingli Ma designed experiments, conducted and coordinated protein purification and crystallization, performed data collection, data processing and initial phasing by molecular replacement, and wrote the manuscript. Y.Y. carried out the construct screening, optimization, purification, and crystallization, and supported manuscript preparation. Yanbin Ma performed construct screening, optimization, purification, and characterization, identified lead peptide for co-crystallization, obtained initial crystals and optimized crystals for diffraction, assisted data collection, and supported ligand binding assay and manuscript preparation. Q. Zhang designed the key mutations for crystallization construct, assisted structure-function relationship pharmacology studies, and supported manuscript preparation. Q. Zhou performed the MD simulation analysis for WT APJR with apelin-13 peptide. Y. Song assisted cell-based functional assay, analyzed data, and generated all cell membranes for radioligand binding assay. Y. Shen designed and supervised the functional analysis and ligand binding assay, analyzed the data, and assisted in manuscript preparation. X.L. performed molecular modeling of  $\kappa$ -OR/dynorphin A and APJR/gp120 V3 complexes, and supported manuscript preparation. X.M. assisted in protein purification and characterization and generated cell membrane for binding assay. C.L. supported the protein purification and manuscript preparation. M.A.H. helped with the X-ray diffraction data processing. G.W.H. helped with structure determination, refinement, and quality check. E.A.S. supported early construct design and purification work. G.S. supported early target identification and biology discovery. S.Z. supervised the MD-related work. R.C.S. initiated and supervised the project, reviewed data, and assisted in manuscript preparation. L.A.H. designed and supervised functional analysis and ligand binding assay, analyzed the data, and assisted in manuscript preparation. W.Z. contributed to construct design and ligand identification, proposed the two-site binding model, and wrote the manuscript. M.Z. conceived the target and assisted in manuscript preparation. F.X. conceived the project, supervised the research, and wrote the manuscript.

## ACKNOWLEDGMENTS

We thank Angela Walker for assistance with the manuscript; Junlin Liu, Xiangxiang Gu, Na Chen, Lu Xue, and the BV Core Facility of iHuman Institute for their support; scientists and colleagues at Amgen Inc., Zhulun Wang, Yaxiong Sun, Jerry Ryan Holder, John G. Allen, Paul J. Dransfield, Jonathan B. Houze, and Philip Tagari, for helpful discussions and support; Jerry Ryan Holder and John G. Allen for originally identifying the potent APJR peptide agonist AMG3054; Mingming Li for ligand supplies; and former colleagues at Amgen Inc., Steve R. Jordan and Samer Chmait, for their contributions to early construct design. We thank the beamline staff at BL41XU of SPring-8 (Hyogo, Japan) for technical help during data collection. We thank Shanghai Supercomputer Center for computational resources. The part of the work conducted at iHuman was supported by the National Natural Science Foundation of China grant 31670736 (F.X.), the National "1000 Talents" young scientist grant (F.X.), Shanghai Pujiang Talent Program grant 16PJ1407300 (S.Z.), and Natural Science Foundation of Shanghai grant 16ZR1448500 (S.Z.).

Received: April 3, 2017  
 Revised: April 7, 2017  
 Accepted: April 24, 2017  
 Published: May 18, 2017

## REFERENCES

Ballesteros, J.A., and Weinstein, H. (1995). Integrated methods for the construction of three-dimensional models and computational probing of structure-function relations in G protein-coupled receptors. *Methods Neurosci.* **25**, 366–428.

Berendsen, H.J.C., Postma, J.P.M., van Gunsteren, W.F., DiNola, A., and Haak, J.R. (1984). Molecular dynamics with coupling to an external bath. *J. Chem. Phys.* **81**, 3684.

Bussi, G., Donadio, D., and Parrinello, M. (2007). Canonical sampling through velocity rescaling. *J. Chem. Phys.* **126**, 014101.

Caffrey, M., and Cherezov, V. (2009). Crystallizing membrane proteins using lipidic mesophases. *Nat. Protoc.* **4**, 706–731.

Caltabiano, G., Gonzalez, A., Cordini, A., Campillo, M., and Pardo, L. (2013). The role of hydrophobic amino acids in the structure and function of the rhodopsin family of G protein-coupled receptors. *Methods Enzymol.* **520**, 99–115.

Carpenter, B., Nehme, R., Warne, T., Leslie, A.G., and Tate, C.G. (2016). Structure of the adenosine A(2A) receptor bound to an engineered G protein. *Nature* **536**, 104–107.

Chandrasekaran, B., Dar, O., and McDonagh, T. (2008). The role of apelin in cardiovascular function and heart failure. *Eur. J. Heart Fail.* **10**, 725–732.

Chavkin, C., and Goldstein, A. (1981). Specific receptor for the opioid peptide dynorphin: structure-activity relationships. *Proc. Natl. Acad. Sci. USA* **78**, 6543–6547.

Cherezov, V., Peddi, A., Muthusubramaniam, L., Zheng, Y.F., and Caffrey, M. (2004). A robotic system for crystallizing membrane and soluble proteins in lipidic mesophases. *Acta Crystallogr. D Biol. Crystallogr.* **60**, 1795–1807.

Chng, S.C., Ho, L., Tian, J., and Reversade, B. (2013). ELABELA: a hormone essential for heart development signals via the apelin receptor. *Dev. Cell* **27**, 672–680.

Choe, H., Farzan, M., Konkil, M., Martin, K., Sun, Y., Marcon, L., Cayabyab, M., Berman, M., Dorf, M.E., Gerard, N., et al. (1998). The orphan seven-transmembrane receptor APJ supports the entry of primary T-cell-line-tropic and dualtropic human immunodeficiency virus type 1. *J. Virol.* **72**, 6113–6118.

Chun, E., Thompson, A.A., Liu, W., Roth, C.B., Griffith, M.T., Katritch, V., Kunken, J., Xu, F., Cherezov, V., Hanson, M.A., et al. (2012). Fusion partner toolchest for the stabilization and crystallization of G protein-coupled receptors. *Structure* **20**, 967–976.

Collman, R., Balliet, J.W., Gregory, S.A., Friedman, H., Kolson, D.L., Nathanson, N., and Srinivasan, A. (1992). An infectious molecular clone of an unusual macrophage-tropic and highly cytopathic strain of human immunodeficiency virus type 1. *J. Virol.* **66**, 7517–7521.

Dassault Systèmes. (2016). BIOVIA, Discovery Studio Modeling Environment (Dassault Systèmes).

Daura, X., Gademann, K., Jaun, B., Seebach, D., van Gunsteren, W.F., and Mark, A.E. (1999). Peptide folding: when simulation meets experiment. *Angew. Chem. Int. Ed.* **38**, 236–240.

Emsley, P., Lohkamp, B., Scott, W.G., and Cowtan, K. (2010). Features and development of Coot. *Acta Crystallogr. D Biol. Crystallogr.* **66**, 486–501.

Essmann, U., Perera, L., Berkowitz, M.L., Darden, T., Lee, H., and Pedersen, L.G. (1995). A smooth particle mesh Ewald method. *J. Chem. Phys.* **103**, 8577–8593.

Falcone, C., Bozzini, S., Schirinzi, S., Buzzi, M.P., Boiocchi, C., Totaro, R., Bondesan, M., and Pelissero, G. (2012). APJ polymorphisms in coronary artery disease patients with and without hypertension. *Mol. Med. Rep.* **5**, 321–325.

Fan, X., Zhou, N., Zhang, X., Mukhtar, M., Lu, Z., Fang, J., DuBois, G.C., and Pomerantz, R.J. (2003). Structural and functional study of the apelin-13 peptide, an endogenous ligand of the HIV-1 coreceptor, APJ. *Biochemistry* **42**, 10163–10168.

Fenalti, G., Giguere, P.M., Katritch, V., Huang, X.P., Thompson, A.A., Cherezov, V., Roth, B.L., and Stevens, R.C. (2014). Molecular control of delta-opioid receptor signalling. *Nature* **506**, 191–196.

Goidescu, C.M., and Vida-Simiti, L.A. (2015). The apelin-APJ system in the evolution of heart failure. *Clujul Med.* **88**, 3–8.

Granier, S., Manglik, A., Kruse, A.C., Kobilka, T.S., Thian, F.S., Weis, W.I., and Kobilka, B.K. (2012). Structure of the delta-opioid receptor bound to naltrindole. *Nature* **485**, 400–404.

- Heckman, K.L., and Pease, L.R. (2007). Gene splicing and mutagenesis by PCR-driven overlap extension. *Nat. Protoc.* 2, 924–932.
- Hess, B., Bekker, H., Berendsen, H.J.C., and Fraaije, J.G.E.M. (1997). LINC: a linear constraint solver for molecular simulations. *J. Comput. Chem.* 18, 1463–1472.
- Hu, L.A., Zhou, T., Hamman, B.D., and Liu, Q. (2008). A homogeneous G protein-coupled receptor ligand binding assay based on time-resolved fluorescence resonance energy transfer. *Assay Drug Dev. Tech.* 6, 543–550.
- Jaakola, V.P., Griffith, M.T., Hanson, M.A., Cherezov, V., Chien, E.Y., Lane, J.R., Ijzerman, A.P., and Stevens, R.C. (2008). The 2.6 angstrom crystal structure of a human A2A adenosine receptor bound to an antagonist. *Science* 322, 1211–1217.
- Jacobson, M.P., Pincus, D.L., Rapp, C.S., Day, T.J., Honig, B., Shaw, D.E., and Friesner, R.A. (2004). A hierarchical approach to all-atom protein loop prediction. *Proteins* 55, 351–367.
- Janecka, A., Fichna, J., and Janocki, T. (2004). Opioid receptors and their ligands. *Curr. Top. Med. Chem.* 4, 1–17.
- Japp, A.G., Cruden, N.L., Barnes, G., van Gemeren, N., Mathews, J., Adamson, J., Johnston, N.R., Denvir, M.A., Megson, I.L., Flapan, A.D., et al. (2010). Acute cardiovascular effects of apelin in humans: potential role in patients with chronic heart failure. *Circulation* 121, 1818–1827.
- Jo, S., Kim, T., Iyer, V.G., and Im, W. (2008). CHARMM-GUI: a web-based graphical user interface for CHARMM. *J. Comput. Chem.* 29, 1859–1865.
- Kabsch, W. (2010). XDS. *Acta Crystallogr. D Biol. Crystallogr.* 66, 125–132.
- Kadoglou, N.P., Lampropoulos, S., Kapelouzou, A., Gkontopoulos, A., Theofilogiannakos, E.K., Fotiadis, G., and Kottas, G. (2010). Serum levels of apelin and ghrelin in patients with acute coronary syndromes and established coronary artery disease—KOZANI study. *Transl. Res.* 155, 238–246.
- Klauda, J.B., Venable, R.M., Freites, J.A., O'Connor, J.W., Tobias, D.J., Mondragon-Ramirez, C., Vorobyov, I., MacKerell, A.D., and Pastor, R.W. (2010). Update of the CHARMM All-ATOM additive force field for lipids: validation on six lipid types. *J. Phys. Chem. B* 114, 7830–7843.
- Langelan, D.N., Bebbington, E.M., Reddy, T., and Rainey, J.K. (2009). Structural insight into G-protein coupled receptor binding by apelin. *Biochemistry* 48, 537–548.
- Madhavi Sastry, G., Adzhigirey, M., Day, T., Annabhimoju, R., and Sherman, W. (2013). Protein and ligand preparation: parameters, protocols, and influence on virtual screening enrichments. *J. Comput. Aided Mol. Des.* 27, 221–234.
- Manglik, A., Kruse, A.C., Kobilka, T.S., Thian, F.S., Mathiesen, J.M., Sunahara, R.K., Pardo, L., Weis, W.I., Kobilka, B.K., and Granier, S. (2012). Crystal structure of the micro-opioid receptor bound to a morphinan antagonist. *Nature* 485, 321–326.
- Masri, B., Knibiehler, B., and Audigier, Y. (2005). Apelin signalling: a promising pathway from cloning to pharmacology. *Cell Signal.* 17, 415–426.
- McCoy, A.J., Grosse-Kunstleve, R.W., Adams, P.D., Winn, M.D., Storoni, L.C., and Read, R.J. (2007). Phaser crystallographic software. *J. Appl. Crystallogr.* 40, 658–674.
- Medhurst, A.D., Jennings, C.A., Robbins, M.J., Davis, R.P., Ellis, C., Winborn, K.Y., Lawrie, K.W., Hervieu, G., Riley, G., Bolaky, J.E., et al. (2003). Pharmacological and immunohistochemical characterization of the APJ receptor and its endogenous ligand apelin. *J. Neurochem.* 84, 1162–1172.
- Murshudov, G.N., Vagin, A.A., and Dodson, E.J. (1997). Refinement of macromolecular structures by the maximum-likelihood method. *Acta Crystallogr. D Biol. Crystallogr.* 53, 240–255.
- Murza, A., Parent, A., Besserer-Offroy, E., Tremblay, H., Karadereye, F., Beaudet, N., Leduc, R., Sarret, P., and Marsault, E. (2012). Elucidation of the structure-activity relationships of apelin: influence of unnatural amino acids on binding, signaling, and plasma stability. *ChemMedChem* 7, 318–325.
- Murza, A., Sainsily, X., Coquerel, D., Cote, J., Marx, P., Besserer-Offroy, E., Longpre, J.M., Laine, J., Reversade, B., Salvail, D., et al. (2016). Discovery and structure-activity relationship of a bioactive fragment of ELABELA that modulates vascular and cardiac functions. *J. Med. Chem.* 59, 2962–2972.
- O'Carroll, A.M., Lolait, S.J., Harris, L.E., and Pope, G.R. (2013). The apelin receptor APJ: journey from an orphan to a multifaceted regulator of homeostasis. *J. Endocrinol.* 219, R13–R35.
- O'Connor, C., White, K.L., Doncescu, N., Didenko, T., Roth, B.L., Czaplicki, G., Stevens, R.C., Wuthrich, K., and Milon, A. (2015). NMR structure and dynamics of the agonist dynorphin peptide bound to the human kappa opioid receptor. *Proc. Natl. Acad. Sci. USA* 112, 11852–11857.
- O'Dowd, B.F., Heiber, M., Chan, A., Heng, H.H., Tsui, L.C., Kennedy, J.L., Shi, X., Petronis, A., George, S.R., and Nguyen, T. (1993). A human gene that shows identity with the gene encoding the angiotensin receptor is located on chromosome 11. *Gene* 136, 355–360.
- Pauli, A., Norris, M.L., Valen, E., Chew, G.L., Gagnon, J.A., Zimmerman, S., Mitchell, A., Ma, J., Dubrulle, J., Reyon, D., et al. (2014). Toddler: an embryonic signal that promotes cell movement via Apelin receptors. *Science* 343, 1248636.
- Pitkin, S.L., Maguire, J.J., Bonner, T.I., and Davenport, A.P. (2010). International union of basic and clinical pharmacology. LXXIV. Apelin receptor nomenclature, distribution, pharmacology, and function. *Pharmacol. Rev.* 62, 331–342.
- Pronk, S., Páll, S., Schulz, R., Larsson, P., Bjelkmar, P., Apostolov, R., Shirts, M.R., Smith, J.C., Kasson, P.M., van der Spoel, D., et al. (2013). GROMACS 4.5: a high-throughput and highly parallel open source molecular simulation toolkit. *Bioinformatics* 29, 845–854.
- Schrödinger. (2016a). Desmond Molecular Dynamics System, D.E. Shaw Research; Maestro-Desmond Interoperability Tools (Schrödinger LLC).
- Schrödinger. (2016b). Prime (Schrödinger, LLC).
- Schwyzler, R. (1977). ACTH: a short introductory review. *Ann. N. Y. Acad. Sci.* 297, 3–26.
- Shi, L., Liapakis, G., Xu, R., Guarneri, F., Ballesteros, J.A., and Javitch, J.A. (2002). Beta2 adrenergic receptor activation. Modulation of the proline kink in transmembrane 6 by a rotamer toggle switch. *J. Biol. Chem.* 277, 40989–40996.
- Shihoya, W., Nishizawa, T., Okuta, A., Tani, K., Dohmae, N., Fujiyoshi, Y., Nureki, O., and Doi, T. (2016). Activation mechanism of endothelin ETB receptor by endothelin-1. *Nature* 537, 363–368.
- Shivakumar, D., Williams, J., Wu, Y., Damm, W., Shelley, J., and Sherman, W. (2010). Prediction of absolute solvation free energies using molecular dynamics free energy perturbation and the OPLS force field. *J. Chem. Theor. Comput.* 6, 1509–1519.
- Smart, O.S., Womack, T.O., Flensburg, C., Keller, P., Paciorek, W., Sharff, A., Vornrhein, C., and Bricogne, G. (2012). Exploiting structure similarity in refinement: automated NCS and target-structure restraints in BUSTER. *Acta Crystallogr. D Biol. Crystallogr.* 68, 368–380.
- Smit, M.J., Vischer, H.F., Bakker, R.A., Jongejan, A., Timmerman, H., Pardo, L., and Leurs, R. (2007). Pharmacogenomic and structural analysis of constitutive G protein-coupled receptor activity. *Annu. Rev. Pharmacol. Toxicol.* 47, 53–87.
- Tamamis, P., and Floudas, C.A. (2013). Molecular recognition of CXCR4 by a dual tropic HIV-1 gp120 V3 loop. *Biophys. J.* 105, 1502–1514.
- Tan, Q., Zhu, Y., Li, J., Chen, Z., Han, G.W., Kufareva, I., Li, T., Ma, L., Fenalti, G., Li, J., et al. (2013). Structure of the CCR5 chemokine receptor-HIV entry inhibitor maraviroc complex. *Science* 341, 1387–1390.
- Vardy, E., Mosier, P.D., Frankowski, K.J., Wu, H., Katritch, V., Westkaemper, R.B., Aube, J., Stevens, R.C., and Roth, B.L. (2013). Chemotype-selective modes of action of kappa-opioid receptor agonists. *J. Biol. Chem.* 288, 34470–34483.
- White, J.F., Noinaj, N., Shibata, Y., Love, J., Kloss, B., Xu, F., Gvozdenovic-Jeremic, J., Shah, P., Shiloach, J., Tate, C.G., et al. (2012). Structure of the agonist-bound neurotensin receptor. *Nature* 490, 508–513.
- Wu, B., Chien, E.Y., Mol, C.D., Fenalti, G., Liu, W., Katritch, V., Abagyan, R., Broun, A., Wells, P., Bi, F.C., et al. (2010). Structures of the CXCR4 chemokine GPCR with small-molecule and cyclic peptide antagonists. *Science* 330, 1066–1071.

- Wu, H., Wacker, D., Mileni, M., Katritch, V., Han, G.W., Vardy, E., Liu, W., Thompson, A.A., Huang, X.P., Carroll, F.I., et al. (2012). Structure of the human kappa-opioid receptor in complex with JDTic. *Nature* *485*, 327–332.
- Xu, F., Wu, H., Katritch, V., Han, G.W., Jacobson, K.A., Gao, Z.G., Cherezov, V., and Stevens, R.C. (2011). Structure of an agonist-bound human A2A adenosine receptor. *Science* *332*, 322–327.
- Zhang, Y., Maitra, R., Harris, D.L., Dhungana, S., Snyder, R., and Runyon, S.P. (2014). Identifying structural determinants of potency for analogs of apelin-13: integration of C-terminal truncation with structure-activity. *Bioorg. Med. Chem.* *22*, 2992–2997.
- Zhang, H., Unal, H., Gati, C., Han, G.W., Liu, W., Zatspein, N.A., James, D., Wang, D., Nelson, G., Weierstall, U., et al. (2015). Structure of the angiotensin receptor revealed by serial femtosecond crystallography. *Cell* *161*, 833–844.
- Zhou, N., Zhang, X., Fan, X., Argyris, E., Fang, J., Acheampong, E., DuBois, G.C., and Pomerantz, R.J. (2003). The N-terminal domain of APJ, a CNS-based coreceptor for HIV-1, is essential for its receptor function and coreceptor activity. *Virology* *317*, 84–94.
- Zou, M.X., Liu, H.Y., Haraguchi, Y., Soda, Y., Tatemoto, K., and Hoshino, H. (2000). Apelin peptides block the entry of human immunodeficiency virus (HIV). *FEBS Lett.* *473*, 15–18.

## STAR★METHODS

## KEY RESOURCES TABLE

REAGENT or RESOURCE	SOURCE	IDENTIFIER
<b>Antibodies</b>		
HA Epitope Tag Antibody, Alexa Fluor 488 conjugate (16B12)	Thermo Fisher Scientific Inc.	Cat# A21287; RRID: AB_1500204
<b>Chemicals, Peptides, and Recombinant Proteins</b>		
EDTA-free complete protease inhibitor cocktail tablets	Roche	Cat# 5056489001
Apelin-13	HD Biosciences	201407Aplin-13
AMG3054	Amgen	N/A
<sup>125</sup> I-Apelin	PerkinElmer	Cat# NEX393
Monoolein (1-Oleoyl- <i>rac</i> -glycerol)	Sigma	Cat# M7765
Cholesterol	Sigma	Cat# C8667
Iodoacetamide	Sigma	Cat# I1149
DDM (N-Dodecyl-B-D-Maltoside)	Anatrace	Cat# D310
CHS (Cholesteryl hemisuccinate)	Sigma	Cat# C6512
CPM (N-[4-(7-diethylamino-4-methyl-3-coumarinyl)phenyl]maleimide)	Invitrogen	Cat# D10251
<b>Critical Commercial Assays</b>		
LANCE Ultra cAMP Kit	Perkin Elmer	Cat# TRF0263
<b>Deposited Data</b>		
APJR-AMG3054 coordinates	PDB, This Study	5VBL
<b>Experimental Models: Cell Lines</b>		
293FT cells	Invitrogen	Cat# R70007
Sf9 cells	Invitrogen	Cat# 11496-015
<b>Oligonucleotides</b>		
pJiF1.1_forward: TAATACGACTCACTATAGGG	GenScript	N/A
pJiF1.1_reverse: TTCAGGTTTCAGGGGGAGGTG	GenScript	N/A
<b>Recombinant DNA</b>		
Human APJ gene	GenScript	N/A
Human APJ mutants	GenScript	N/A
pJiF1.1 vector	Amgen	N/A
<b>Software and Algorithms</b>		
Prism v.6.0	GraphPad Software Inc.	N/A
Schrödinger Suite 2016-1	Schrödinger	<a href="https://www.schrodinger.com/">https://www.schrodinger.com/</a>
Discovery Studio 2017	Dassault Systèmes BIOVIA	<a href="http://accelrys.com/">http://accelrys.com/</a>
Gromacs 5.1.2	Gromacs	<a href="http://www.gromacs.org/">http://www.gromacs.org/</a>
Pymol 1.7.0.0	Schrödinger	<a href="http://www.pymol.org/">http://www.pymol.org/</a>
XDS	<a href="#">Kabsch, 2010</a>	Xds.mpimf-heidelberg.mpg.de
Phaser	<a href="#">McCoy et al., 2007</a>	<a href="https://www.phenix-online.org">https://www.phenix-online.org</a>
Buster	<a href="#">Smart et al., 2012</a>	<a href="https://www.globalphasing.com/buster">https://www.globalphasing.com/buster</a>
Coot	<a href="#">Emsley et al., 2010</a>	<a href="http://www2.mrc-lmb.cam.ac.uk/personal/pemsley/coot">http://www2.mrc-lmb.cam.ac.uk/personal/pemsley/coot</a>
<b>Other</b>		
96-well Polypropylene plates	Costar	Cat# 3357
96 well assay plate	Costar	Cat# 3694
UniFilter-96 GF/B PEI Coated Plate	Perkin Elmer	Cat# 6005277
Cell harvester	Perkin Elmer	FilterMate™ Universal Harvester
FreeStyle 293 Expression Medium	Life Technologies	Cat# 12338-026

(Continued on next page)

**Continued**

REAGENT or RESOURCE	SOURCE	IDENTIFIER
Sf9 expression medium	Expression Systems	Cat# 96-001-01
Forsklin	Sigma	Cat# F6886
TALON IMAC resin	Clontech	Cat# 635507
IBMX	Sigma	Cat# I5879

**CONTACT FOR REAGENT AND RESOURCE SHARING**

Further information and requests for reagents may be directed to, and will be fulfilled by the lead contact Fei Xu ([xufei@shanghaitech.edu.cn](mailto:xufei@shanghaitech.edu.cn)).

**METHOD DETAILS****Cloning and Expression**

The WT human APJR gene was synthesized by GenScript with codon optimization for expression in Sf9, and then cloned into a modified pFastBac1 vector (Invitrogen) containing an expression cassette with an HA signal sequence followed by a Flag tag at the N-terminus, and a pT7E1 recognition site followed by a 10× His tag at the C-terminus. Six amino acids were deleted from the N-terminus (residues 1–6), and 50 residues were truncated from the C-terminus (residues 331–380). In ICL3, residues 230–242 were replaced with M1-E54 of rubredoxin (Chun et al., 2012) by overlap extension PCR (Heckman and Pease, 2007). Two mutations C325L and C326M were introduced to inhibit the palmitoylation of APJR and T177N was introduced to remove a glycosylation site. Model-based mutations V117A and W261K were further introduced to stabilize APJR at the inactive state for conformational homogeneity; these two mutations were designed in the presence of three inactive-state APJR homology models built on the crystal structures of AT1R (PDB ID: 4YAY), δ-OR (4N6H), and the nociceptin orphanin FQ peptide receptor (4EA3). Recombinant baculoviruses were generated using the Bac-to-Bac System (Invitrogen), and Sf9 insect cells at a density of  $2-3 \times 10^6$  cells/ml were infected with virus at a multiplicity of infection of 5. Infected cells were harvested after 48 h incubation, and the cell pellets were stored at  $-80^\circ\text{C}$ .

**Protein Purification**

Cells from 2 l of P2 virus infected insect cell culture were re-suspended with 100 ml of hypotonic buffer (10 mM HEPES pH 7.5, 10 mM  $\text{MgCl}_2$ , 20 mM KCl, 2 tablets of protease inhibitor cocktail (Roche, Catalog# 4693132001) in a 100 ml Kimble™ Kontes™ Dounce. After centrifugation (rotor Beckman Coulter Ti45, 40 min at 35,000 rpm and  $4^\circ\text{C}$ ), the pellet was washed twice with 100 ml of high salt buffer (10 mM HEPES pH 7.5, 10 mM  $\text{MgCl}_2$ , 20 mM KCl, 1 M NaCl, 1 tablet of protease inhibitor cocktail (Roche, Catalog# 4693132001)). The washed membrane was resuspended in 100 ml of low salt buffer (10 mM HEPES pH 7.5, 10 mM  $\text{MgCl}_2$ , 20 mM KCl) containing 30% glycerol supplemented with 2 mg/ml iodoacetamide and incubated at  $4^\circ\text{C}$  for 20 min. The receptor was extracted by adding another 100 ml of solubilization buffer (100 mM HEPES pH 7.5, 1.6 M NaCl, 2% (w/v) DDM, 0.4% (w/v) cholesterol hemisuccinate) at 1:1 ratio by volume and supplemented with 15mM imidazole, followed by incubation at  $4^\circ\text{C}$  for 2 h. After centrifugation (rotor Beckman Coulter Ti45, 40 min at 35,000 rpm and  $4^\circ\text{C}$ ), the supernatant was mixed with 1.4 ml of talon superflow metal affinity resin and incubated at  $4^\circ\text{C}$  for another 1.5 h. The mixture was packed in an Econo-Pac disposable chromatography column by gravity and washed with 14 column volumes of buffer (25 mM HEPES pH 7.5, 500 mM NaCl, 5% glycerol, 0.05% (w/v) DDM, 0.01% (w/v) cholesterol hemisuccinate, 30 mM imidazole, 10 mM  $\text{MgCl}_2$ , 8 mM ATP). The receptor was eluted with 2.5 column volumes of buffer (25 mM HEPES pH 7.5, 500 mM NaCl, 5% glycerol, 0.01% (w/v) DDM, 0.002% (w/v) cholesterol hemisuccinate, 200 mM imidazole). 3.5 ml elution containing abundant of purified APJR receptor was supplemented with 17.5  $\mu\text{l}$  of 500  $\mu\text{M}$  AMG3054 from 100 mM stock in  $\text{H}_2\text{O}$  and concentrated in a 100 kDa molecular mass cut-off concentrator from Sartorius to 30–40 mg/ml. Protein purity, monodispersity were estimated by SDS–PAGE and analytical size-exclusion chromatography (aSEC).

**Crystallization**

Purified and concentrated APJR-AMG3054 complex samples were reconstituted into lipidic cubic phase (LCP) by mixing with molten lipid in a mechanical syringe mixer (Caffrey and Cherezov, 2009). The APJR-AMG3054 complex-LCP mixture contained 40% (w/w) protein solution, 54% (w/w) monoolein (Sigma) and 6% (w/w) cholesterol (AvantiPolar Lipids). After the transparent LCP was achieved, crystallization trials were performed in 96-well glass sandwich plates (Cherezov et al., 2004) (NOVA), 40 nl drops and 800 nl precipitant solution were mixed in each well, using an NT8-LCP crystallization robot (Formulatrix), and sealed with a glass coverslip. Protein reconstitution in LCP and crystallization was conducted at room temperature ( $20-22^\circ\text{C}$ ). The plates were stored and imaged in an imager (RockImager 1000, Formulatrix) at  $20^\circ\text{C}$ . Crystals started to appear around 1 d after incubation at  $20^\circ\text{C}$  and reached maximum size  $\sim 100 \mu\text{m}$  within 1 wk in 100 mM MES pH 6.1, 26% PEG500 DME, 125 mM  $\text{MgCl}_2$ , 100 mM NaCl, 500  $\mu\text{M}$  AMG3054. Crystals were harvested directly from the LCP drop with 100  $\mu\text{m}$  MiTeGen micromounts and flash frozen in liquid nitrogen.

### Data Collection and Structure Determination

X-ray diffraction data were collected at the SPring-8 beam line 41XU (Hyogo, Japan) with a Pilatus3 6M detector (X-ray wavelength 1.0000 Å). The crystals were exposed with a 12x9 μm beam for 0.2 s and 0.2° oscillation per frame. In order to prevent radiation damage, data were collected in wedges of 10–30° with attenuation at 590 μm before moving onto a different site either on the same crystal or on a new crystal. The data from 9 crystals of APJR-AMG3054 complex were integrated and scaled using XDS (Kabsch, 2010). The initial molecular replacement was performed with PHASER (McCoy et al., 2007) using the 3.4 Å δ-OR receptor structure (PDB ID: 4EJ4) with T4L removed and rubredoxin (PDB ID: 1IRO) domains as independent search models. Refinement of the APJR-AMG3054 complex was performed with REFMAC5 (Murshudov et al., 1997)\_ENREF\_27 and autoBUSTER (Smart et al., 2012)\_ENREF\_28 followed by manual examination and rebuilding of the refined coordinates in the program COOT (Emsley et al., 2010) using both  $|2F_o - F_c|$  and  $|F_o - F_c|$  maps. Residues 7–18 of the N-terminus are disordered and not visible in the electron density maps. They were not modeled. The final model contains 297 residues (19–229 and 243–330) of APJR and residues 1 to 54 of rubredoxin. One zinc ion from rubredoxin is also modeled (Tan et al., 2013). The data collection and refinement statistics are shown in Table S1.

### Mutagenesis and Generation of Cell Lines

Mutations were designed into three categories: 1) 18 binding site mutations were based on the AT1R (PDB ID: 4YAY)-based APJR homology model; 2) 13 mutations were based on the APJR-AMG3054 crystal structure to cover 4 more residues inside the binding pockets and 9 more residues on APJR ECD; 3) 6 constructs containing back mutations were based on the crystallized construct. HA-tagged human full length APJR in pJIF1.1 vector was used as a template to generate APJR mutant bacmids by PCR-based mutagenesis. The resulting bacmids were used to generate baculovirus by infecting insect Sf9 cells according to the standard protocol. For APJR transient expression, 293FT cells were transduced with the above recombinant baculovirus. Cells were cultured in FreeStyle™ 293 Expression medium in suspension and grown to a cell density of 1–2 × 10<sup>6</sup> viable cells/ml before transduction. Then cells were diluted to a density of 0.4 × 10<sup>6</sup> viable cells/ml before adding baculovirus to 20% of final volume. Cells were incubated at 37 °C incubator containing 5% CO<sub>2</sub> on an orbital shaker platform rotating at 130 rpm for 24 h before harvest for functional assay or membrane preparation. Receptor (WT and mutants) cell surface expression was checked by FACS using Alexa 488 conjugated anti-HA antibody, while total membrane receptor levels were analyzed by Western blot using anti-HA antibody.

### cAMP Assay

APJR function was measured based on intracellular cAMP levels using Lance Ultra cAMP kit (Perkin Elmer) according to manufacturer's protocol. Briefly, 10 μl of 2000 cells in assay buffer (HBSS buffer pH 7.4 with 5 mM HEPES, 0.1% BSA and 0.5 mM IBMX) were added to each well of 96-well assay plate, and stimulated with 10 μl of various concentrations of compounds with 2.5 μM forskolin for 30 min at 37 °C. Then 10 μl of 4 × Eu-cAMP and 10 μl of 4 × Ulight-Anti-cAMP working solutions were added to each well sequentially. The assay plate was incubated at RT for 1 h before reading with Envision plate reader using configurations recommended by manufacturer. All signals (ratio of RFU 665 nm/RFU 615 nm) were fit to a sigmoidal dose-response model using GraphPad Prism 6 software. Data were presented as Mean and SEM of three independent experiments in duplicates.

### APJR Saturation Binding

Cell membranes from 293FT suspension cells were prepared as described previously (Hu et al., 2008). The membrane preparations were aliquoted and stored in -80 °C freezer. The membrane protein concentration was determined with BCA kit using BSA as standard. Radioligand saturation binding assays were performed in 96-well filtration plate. WT or mutant APJR membrane (3 μg) were incubated with various concentrations of [<sup>125</sup>I]-Apelin-13 in the ligand binding buffer (50 mM HEPES pH 7.4, 5 mM MgCl<sub>2</sub>, 1 mM CaCl<sub>2</sub>, 0.2% BSA) in a total volume of 120 μl. Following incubation at RT for 2 h with gentle shanking, the reaction mixtures were then transferred to UniFilter GF/B filtration Plate (PEI Coated, PE). The plate was washed three times immediately with ice-cold washing buffer (50 mM HEPES pH 7.4, 500 mM NaCl, 0.1% BSA) using Perkin Elmer FilterMate™ Universal Harvester. After the plates were dried at 37 °C for 2 h, scintillation cocktail (50 μl) was added to each well, and radioactivity was determined by MicroBeta Trilux. Non-specific binding was determined in the presence of 100 nM cold apelin-13 in the reaction mixture. All data were fit to one-site specific binding model using GraphPad Prism 6 software. K<sub>d</sub> and B<sub>max</sub> were calculated from the best-fit values of the specific binding. Data were presented as Mean and SEM of three or more independent experiments in duplicates.

### Molecular Dynamics Simulations of APJR with Endogenous Peptide Apelin-13

In all simulations, the APJR receptor was embedded in a hydrated lipid bilayer with all atoms, including those in the lipids and water, represented explicitly. To simulate the apelin-13 and APJR complex in the no-fusion no-mutation background, the crystal structure was initially prepared using the Protein Preparation Wizard (Schrödinger, Inc.) (Madhavi Sastry et al., 2013), followed by five back mutations (T177N, C325L, C326M, V117<sup>3.40</sup>A and W261<sup>6.48</sup>K) to the original residue using the Residue and Loop Mutation functionality in BioLuminate (Schrödinger, Inc.), and the missing loop of ICL3 filled by Prime (Schrödinger, Inc.). The initial conformation of apelin-13 with APJR was obtained by gradually mutating AMG3054 to apelin-13 by multiple rounds of single residue modification/mutation and energy minimization using the Protein Preparation Wizard (Schrödinger, Inc.).

Hydrogen atoms were added using Maestro (Schrödinger, Inc.) while protonation states were assigned using PROPKA. Prepared APJR receptor-ligand complexes were inserted into a pre-equilibrated POPC lipid bilayer and solvated with water using the CHARMM-GUI interface (Jo et al., 2008). Sodium and chloride ions were added to neutralize the system and to reach a final

concentration of 150 mM in solution. The simulation box initially measured 91 Å × 90 Å × 120 Å and contained one APJR receptor, one apelin-13 peptide, 155 lipid molecules, 39 sodium ions, 52 chloride ions and approximately 15,077 water molecules, for a total of approximately 71,348 atoms. We used the CHARMM36 parameter (Klauda et al., 2010) set for protein molecules, lipid molecules, and salt ions, and the CHARMM TIP3P model for water. All MD simulations were conducted using Gromacs 5.1.2 accelerated with GPU (Pronk et al., 2013). All bonds involving hydrogen atoms were constrained using LINCS algorithm (Hess et al., 1997). The particle mesh Ewald (PME) method (Essmann et al., 1995) was used to treat long-range electrostatic interactions. Neighbor lists were updated every 20 time steps. Van der Waals interactions and real space Coulombic interactions were calculated with a cutoff of 12 Å. The entire system was first relaxed using the steepest descent energy minimization, followed by slow heating of the system to 300 K with harmonic restraints applied to the APJR receptor, apelin-13, and the lipids. The restraints to the main chain of the protein and the peptide ligand were reduced gradually to zero by equilibration steps of 50 ns in total to equilibrate the lipid bilayer and the solvent. Finally, the system was run without restraints, with a time step of 2 fs in the NPT ensemble at 300 K and 1 bar using a v-rescale thermostat (Bussi et al., 2007) and Berendsen barostat (Berendsen et al., 1984), respectively. Gromacs utility `g_cluster` was used to cluster the frames by the gromos method (Daura et al., 1999).

### Molecular Modeling of $\kappa$ -OR-Dynorphin A Complex

The initial structures of  $\kappa$ -OR and N-terminal part of dynorphin A (Y1-G3) were extracted from the previously published " $\kappa$ -OR -1" model (O'Connor et al., 2015). The remaining part of dynorphin A (F4-Q17) was modeled manually in Discovery Studio (Dassault Systèmes, 2016) to adjust the peptide orientation based on that of AMG3054. The model was minimized with Prime in Schrödinger (Schrödinger, 2016b; Jacobson et al., 2004), with VSGB solvation model and OPLS3 force field. Then it was embedded in POPC membrane with TIP3P explicit water model and counterions under the OPLS3 force field. MD simulation was performed on the system with Desmond in Schrödinger (Schrödinger, 2016a; Shivakumar et al., 2010). The system was relaxed before simulation with default protocol. 20 ns simulation was performed in the NPT ensemble, at temperature of 300 K and pressure of 1 bar. After that, the complex conformations were clustered by the backbone RMSD. The complex conformation with lowest interaction energy from the largest cluster was selected as the final model.

### Molecular Modeling of APJR-gp120 V3 Loop Complex

The gp120 V3 loop sequence "CTRPNNNTRRRRLSIGPGRAFYARRNIIGDIRQAHC" used here was from HIV-1 89.6 strain (Collman et al., 1992) as APJR has been reported to support its entry as a coreceptor (Choe et al., 1998; Zhou et al., 2003). The initial model of the APJR-gp120 V3 loop complex was built via homology modeling in Discovery Studio (Dassault Systèmes, 2016), with both our APJR-AMG3054 structure and previously published CXCR4/gp120 V3 loop complex model (Tamamis and Floudas, 2013) as templates. Then it was embedded in POPC membrane with TIP3P explicit water model and counterions under the OPLS3 force field. Molecular dynamics simulation was performed on the system with Desmond in Schrödinger (Schrödinger, 2016a; Shivakumar et al., 2010). The system was relaxed before simulation with default protocol. 20 ns simulation was performed in the NPT ensemble, at temperature of 300 K and pressure of 1 bar. After that, the complex conformations were clustered by the backbone RMSD. The complex conformation with lowest interaction energy from the largest cluster was selected as the final model.

## QUANTIFICATION AND STATISTICAL ANALYSIS

Concentration-response curves for cAMP were presented as signal ratio of 665 nm/615 nm as indicated. Concentration-response curves were fit to a non-linear regression (four parameters) model to determine  $EC_{50}$  in Prism (v. 6.0, GraphPad Software Inc., San Diego, CA), as indicated. Radioligand binding data were fit to a one-site specific binding model to determine  $K_d$  in Prism (v. 6.0, GraphPad Software Inc., San Diego, CA), as indicated.

## DATA AND SOFTWARE AVAILABILITY

The accession number for the structure reported in this paper is PDB: [5VBL].